Journal of Solid Mechanics Vol. 14, No. 1 (2022) pp. 1-16
DOI: 10.22034/jsm.2019.585582.1401

Static and Dynamic Stability Analysis of Thick CNT Reinforced Beams Resting on Pasternak Foundation Under Axial and Follower Forces

M. Hosseini [1], A. Ghorbanpour Arani [2,3 *], M. Karamizadeh[1], Sh. Niknejad [2], A. Hosseinpour [4]

[1]*Department of Mechanical Engineering, Sirjan University of Technology, Sirjan, Iran*
[2]*Faculty of Mechanical Engineering, University of Kashan, Kashan, Iran*
[3]*Institute of Nanoscience &Nanotechnology, University of Kashan, Kashan, Iran*
[4]*Department of Mechanical Engineering and Engineering science, University of North Carolina at Charlotte, United States*

Received 1 September 2021; accepted 14 November 2021

ABSTRACT

In this paper, a numerical solution is presented for static and dynamic stability analysis of carbon nanotube (CNT) reinforced beams resting on Pasternak foundation. The beam is considered to be exposed to compressive axial and follower forces at its free end. The beam is modeled based on the Reddy's third order shear deformation theory and governing equations and external boundary conditions are derived using Hamilton's principle. The set of governing equations and boundary conditions are solved numerically using differential quadrature method. Convergence and accuracy of results are confirmed and effect of various parameters on the stability region of the beam is investigated including volume fraction and distribution of CNTs, width and thickness of the beam and elastic and shear coefficients of the foundation.

Keywords: Dynamic stability; Follower force; Carbon nanotube; Pasternak foundation.

1 INTRODUCTION

AXIAL compressive load leads to static instability of structures but dynamic instability in structures (beams, pipes, plates and shells) may be created due to internal [1-4] or external [5-8] fluid flows or follower force. Dynamic stability analysis of structures subjected to follower forces is of practical importance in such fields as aerospace, mechanical and civil engineering. Due to this importance, many researchers focused on the dynamic stability analysis of structures. Irie et al. [9] used Timoshenko beam theory and studied vibration and dynamic stability analysis of non-uniform beams subjected to follower force. They studied variation of cross section of the beam on the critical load. Using finite element method, Park [10] focused on the dynamic stability analysis of a free-free Timoshenko beam under a controlled follower force. He studied effect of feedback gain on the stability region

*Corresponding author. Tel.: +98 913 1626594; Fax.: +98 361 5559930.
E-mail address: aghorban@kashanu.ac.ir (A.Ghorbanpour Arani)

of the beam. Using Timoshenko beam element, Lien and Jeng [11] investigated dynamic stability of a bimodulus beam subjected to a follower force. Dynamic stability analysis of a tapered cantilever beam resting on a foundation subjected to a follower force was studied by Lee [12]. He focused on the effect of internal damping of the beam and damping of the foundation on the critical load. Takahashi and Yoshioka [13] used transfer matrix method (TMM) and focused on vibration and stability analysis of a stepped beam with internal span subjected to follower force. Using transfer matrix method and Timoshenko beam theory, Takahashi [14] studied vibration and stability analysis of non-uniform cracked beams subjected to follower force. Young and Juan [15] used Ritz-Galerkin method and studied stability and response of fluttered beams subjected to random follower forces. Djondjorov and Vassilev [16] employed theory Timoshenko beam theory and focused on the dynamic stability analysis of cantilever beams resting on Winkler foundation subjected to tangential follower force. Goyal and Kapania [17] studied dynamic stability of laminated beams subjected to non-conservative loads. Li [18] presented an exact solution for stability analysis of non-uniform columns under the combined action of concentrated follower forces and variably distributed loads. He considered some especial cases of variation in cross section which can be solved analytically. Bending-torsional flutter analysis of wings with an attached mass subjected to a follower force was studied by Fazelzadeh et al. [19]. Wang [20] focused on the stability analysis of pipes conveying fluid subjected to distributed follower forces. He showed that depending on the properties and velocity of the fluid and value of the follower force, either dynamic or static instabilities can happen. Using adomian decomposition method (ADM), Mao and Wattanasakulpong [21] studied effect of conservative and non-conservative axial forces on the vibration and stability analysis of a double-beam system interconnected by an elastic foundation. They studied effect of stiffness of internal springs on the stability regions of the system. Bahaadini et al. [22] studied nonlocal and surface effects on the dynamic stability analysis of cantilever nanotubes conveying fluid subjected to follower force. They confirmed that surface effect leads to increase in stability of the nanotubes. Using a modified nonlocal elasticity theory and employing Galerkin method, Bahaadini and Hosseini [23] studied flutter and divergence analysis of cantilever carbon nanotubes conveying fluid, embedded in viscoelastic foundation and subjected to an axial compressive load. They concluded that stability boundaries of the CNT are strongly dependent on the small-scale coefficient and surface effects. Due to their unique mechanical properties, many researchers focused on the effect of CNTs and graphene nanoplatelets on the mechanical behavior of structures. Mohammadimehr et al. [24] employed modified couple stress theory and presented an exact solution for free and forced vibration analysis of viscoelastic FG-CNT reinforced micro composite beams. Arefi et al. [25] employed a two-variable sinusoidal shear deformation theory within a nonlocal elasticity theory and studied free vibration analysis of functionally graded polymer composite nanoplates reinforced with graphene nanoplatelets resting on a Pasternak foundation. Using first-order shear deformation theory, Arefi et al. [26] focused on the two-dimensional thermo-elastic analysis of CNT reinforced cylindrical pressure vessels subjected to inner and outer pressure under a temperature rise. This work was repeated and improved using the third-order shear deformation theory by Mohammadi et al. [27]. By employing the first-order shear deformation theory and the nonlocal elasticity theory, Arefi et al. [28] presented a parametric study on the bending analysis of functionally graded polymer composite curved beams reinforced by graphene nanoplatelets resting on a Pasternak foundation. Because of their high accuracy, higher order shear deformation theories have been used by many authors in the recent years to study mechanical analysis of various types of structures [29-33].

In this paper, Reddy's third order beam theory is employed and static and dynamic stability analysis of CNT-reinforced cantilever beams resting on Pasternak foundation subjected to axial and follower forces are studied. Governing equations and boundary conditions are solved numerically using differential quadrature method. Convergence and accuracy of the presented solution are examined and effect of volume fraction and distribution of CNTs, geometrical parameters and elastic and shear coefficients of the foundation on the stability boundaries are investigated. There are many papers regarding stability analysis of beams subjected to axial or follower forces. But in this paper stability regions are derived in the presence of both axial and follower forces which can be considered as the novelty of the presented work. Also, Reddy's third order shear deformation theory is employed in this paper which makes results more accurate in comparison with previous works which used Euler-Bernoulli or Timoshenko beam theories.

2 GOVERNING EQUATIONS

As depicted in Fig. 1, a cantilevered CNT-reinforced beam of length L, with b and thickness h is considered. The beam is exposed to an axial (Q) and a follower (P) force applied at the free end. According to the extended rule of mixture, elastic (E_{11}) and shear (G_{12}) moduli of the beam can be estimated as [34]:

$$E_{11}(z)=\eta_1 V_{CNT}(z)E_{11}^{CNT}+V_m(z)E^m$$
$$\frac{\eta_3}{G_{12}(z)}=\frac{V_{CNT}(z)}{G_{12}^{CNT}}+\frac{V_m(z)}{G^m} \quad (1)$$

In which E_{11}^{CNT}, G_{12}^{CNT} and V_{CNT} are elastic and shear moduli and volume fraction of the carbon nanotubes, respectively and E^m, G^m and V_m=1-V_{CNT} indicate corresponding ones of the isotropic matrix. It is extremely difficult to achieve perfect bond between the CNTs and isotropic polymer matrix. So, a certain part of interactive force between them is reduced. Therefore CNT efficiency parameters (η_1 and η_3) are introduced in Eq. (1) to consider the above incomplete interfacial interactions by matching the elastic modulus of CNTs from the molecular dynamics (MD) results with the numerical ones obtained from the rule of mixture [34].

Also, density (ρ) and Poisson's ratio (υ) of the beam can be calculated as [34]:

$$\rho(z)=V_{CNT}(z)\rho^{CNT}+V_m(z)\rho^m$$
$$\upsilon=V_{CNT}(z)\upsilon_{12}^{CNT}+V_m(z)\upsilon^m \quad (2)$$

where v_{12}^{CN} and ρ^{CNT} are Poisson's ratio and density of CNT, respectively and v^m and ρ^m are corresponding ones of the isotropic matrix.

The CNT distribution is functionally graded by linearly varying the volume fraction of the CNT in thickness direction. Various types of distribution of CNTs are considered including UD, FG-V, FG-O and FG-X. For these types of distribution which are depicted in Fig. 2, volume fractions of CNTs are given by

$$\begin{aligned} &UD: && V_{CNT}(z)=V_{CNT}^*\\ &FG-V: && V_{CNT}(z)=\left(1+\frac{2z}{h}\right)V_{CNT}^*\\ &FG-O: && V_{CNT}(z)=2\left(1-\frac{2|z|}{h}\right)V_{CNT}^*\\ &FG-X: && V_{CNT}(z)=4\frac{|z|}{h}V_{CNT}^* \end{aligned} \quad (3)$$

According to the Reddy's third order shear deformation beam theory, the displacement field is considered as [35]:

$$u^z(x,z,t)=u(x,t)+z\,\phi(x,t)-c_1z^3\left[\phi(x,t)+\frac{\partial w(x,t)}{\partial x}\right]$$
$$w^z(x,z,t)=w(x,t) \quad (4)$$

where c_1= 4/(3h^2), u^z and w^z show the components of displacement along x and z directions, respectively. u and w indicate corresponding components of displacement at the middle axis (z= 0) and ϕ is rotation about y axis. Using strain-displacement relations, nonzero components of strain can be stated as:

$$\varepsilon_x=\frac{\partial u^z}{\partial x}=\frac{\partial u}{\partial x}-c_1z^3\frac{\partial^2 w}{\partial x^2}+\left(z-c_1z^3\right)\frac{\partial\phi}{\partial x}$$
$$\gamma_{xz}=\frac{\partial u^z}{\partial z}+\frac{\partial w^z}{\partial x}=\left(1-3c_1z^2\right)\left(\frac{\partial w}{\partial x}+\phi\right) \quad (5)$$

Based on the Hooke's law, components of stress can be written as [36]:

$$\sigma_x = E_{11}\varepsilon_x = E_{11}\left[\frac{\partial u}{\partial x} - c_1 z^3 \frac{\partial^2 w}{\partial x^2} + \left(z - c_1 z^3\right)\frac{\partial \phi}{\partial x}\right]$$
$$\sigma_{xz} = G_{12}\gamma_{xz} = G_{12}\left(1 - 3c_1 z^2\right)\left(\frac{\partial w}{\partial x} + \phi\right) \tag{6}$$

According to the Hamilton's principle, considering δ as variational operator and $[t_1,t_2]$ as a desired time interval, the set of governing equations and boundary conditions can be derived using following relation:

$$\int_{t_1}^{t_2}\left(\delta T - \delta U + \delta W_{nc}\right)dt = 0 \tag{7}$$

In which T, U and W_{nc} are kinetic energy, potential energy and work done by external non-conservative forces. The kinetic energy can be stated as follow:

$$T = \frac{1}{2}\iiint_V \rho\left[\left(\frac{\partial u^z}{\partial t}\right)^2 + \left(\frac{\partial v^z}{\partial t}\right)^2 + \left(\frac{\partial w^z}{\partial t}\right)^2\right]dV \tag{8}$$

In which V is volume of the beam. The potential energy of the beam and foundation can be calculated as [12, 36, 37]:

$$U = \frac{1}{2}\iiint_V\left(\sigma_x\varepsilon_x + \sigma_{xz}\gamma_{xz}\right)dV - \frac{1}{2}\int_0^L\left[P\left(\frac{\partial w}{\partial x}\right)^2 + Q\left(\frac{\partial w}{\partial x}\right)^2\right]dx + \frac{1}{2}\int_0^L\left[k_w w^2 + k_G\left(\frac{\partial w}{\partial x}\right)^2\right]dx \tag{9}$$

where the first part is potential energy of the beam, the second part is additional potential energy of the beam created due to the compressive axial and follower forces and the third part is additional potential energy created by the Pasternak foundation. It is worth mentioning that reaction of an elastic foundation is a conservative force which can be considered in the potential energy or in the work done by external forces.

The transverse component of the follower force is a non-conservative force and no potential energy can be defined for this force component. The virtual work of this transverse component of the follower force can be expressed as [12]:

$$\delta W_{\text{nc}} = -\left(P\frac{\partial w}{\partial x}\delta w\right)\Big|_{x=L} \tag{10}$$

Substituting Eqs. (4)-(6) and (8)-(10) in Eq. (7), the set of governing equations can be written as:

$$\frac{\partial N_x}{\partial x} - I_0\frac{\partial^2 u}{\partial t^2} - J_3\frac{\partial^2 \phi}{\partial t^2} + c_1 I_3\frac{\partial^3 w}{\partial t^2 \partial x} = 0$$
$$c_1\frac{\partial^2 P_x}{\partial x^2} + \frac{\partial Q_x}{\partial x} - 3c_1\frac{\partial R_x}{\partial x} - \frac{P+Q-k_G}{b}\frac{\partial^2 w}{\partial x^2} - \frac{k_w}{b}w - c_1 I_3\frac{\partial^3 u}{\partial t^2 \partial x} - I_0\frac{\partial^2 w}{\partial t^2} + c_1^2 I_6\frac{\partial^4 w}{\partial t^2 \partial x^2} - J_5\frac{\partial^3 \phi}{\partial t^2 \partial x} = 0 \tag{11}$$
$$-c_1\frac{\partial P_x}{\partial x} + \frac{\partial M_x}{\partial x} + 3c_1 R_x - Q_x - J_3\frac{\partial^2 u}{\partial t^2} + J_5\frac{\partial^3 w}{\partial t^2 \partial x} - J_1\frac{\partial^2 \phi}{\partial t^2} = 0$$

In which

$$J_1 = I_2 - 2c_1 I_4 + c_1^2 I_6 \quad J_3 = I_1 - c_1 I_3 \quad J_5 = c_1 I_4 - c_1^2 I_6 \quad I_i = \int_{-\frac{h}{2}}^{\frac{h}{2}} z^i \rho(z)dz \quad i = 0,1,2,3,4,6 \tag{12a}$$

$$N_x=\int_{-\frac{h}{2}}^{\frac{h}{2}}\sigma_x dz \quad M_x=\int_{-\frac{h}{2}}^{\frac{h}{2}}z\,\sigma_x dz \quad P_x=\int_{-\frac{h}{2}}^{\frac{h}{2}}z^3\sigma_x dz \quad Q_x=\int_{-\frac{h}{2}}^{\frac{h}{2}}\sigma_{xz} dz \quad R_x=\int_{-\frac{h}{2}}^{\frac{h}{2}}z^2\sigma_{xz} dz \tag{12b}$$

Also, boundary conditions can be written as:

$$x=0:\ \ u=0\ \ \ w=0\ \ \ \frac{\partial w}{\partial x}=0\ \ \ \phi=0 \tag{13a}$$

$$\begin{aligned}&x=L:\ \ N_x=0\ \ \ c_1P_x-M_x=0\ \ \ c_1P_x=0\\&-\frac{P}{b}\frac{\partial w}{\partial x}-c_1\frac{\partial P_x}{\partial x}+3c_1R_x-Q_x+\frac{P+Q-k_G}{b}\frac{\partial w}{\partial x}-c_1^2I_6\frac{\partial^3 w}{\partial t^2\partial x}+c_1I_3\frac{\partial^2 u}{\partial t^2}+J_5\frac{\partial^2\phi}{\partial t^2}=0\end{aligned} \tag{13b}$$

Substituting Eq. (6) in Eq. (12b) leads to

$$\begin{aligned}N_x&=A_{11}\frac{\partial u}{\partial x}+\left(B_{11}-c_1D_{11}\right)\frac{\partial\phi}{\partial x}-c_1D_{11}\frac{\partial^2 w}{\partial x^2}\\M_x&=B_{11}\frac{\partial u}{\partial x}+\left(C_{11}-c_1F_{11}\right)\frac{\partial\phi}{\partial x}-c_1F_{11}\frac{\partial^2 w}{\partial x^2}\\P_x&=D_{11}\frac{\partial u}{\partial x}+\left(F_{11}-c_1H_{11}\right)\frac{\partial\phi}{\partial x}-c_1H_{11}\frac{\partial^2 w}{\partial x^2}\\Q_x&=\left(A_{12}-3c_1C_{12}\right)\left(\frac{\partial w}{\partial x}+\phi\right)\\R_x&=\left(C_{12}-3c_1F_{12}\right)\left(\frac{\partial w}{\partial x}+\phi\right)\end{aligned} \tag{14}$$

In which

$$\begin{aligned}&A_{11}=\int_{-\frac{h}{2}}^{\frac{h}{2}}E_{11}(z)dz \qquad B_{11}=\int_{-\frac{h}{2}}^{\frac{h}{2}}zE_{11}(z)dz \qquad C_{11}=\int_{-\frac{h}{2}}^{\frac{h}{2}}z^2E_{11}(z)dz\\&D_{11}=\int_{-\frac{h}{2}}^{\frac{h}{2}}z^3E_{11}(z)dz \quad F_{11}=\int_{-\frac{h}{2}}^{\frac{h}{2}}z^4E_{11}(z)dz \quad H_{11}=\int_{-\frac{h}{2}}^{\frac{h}{2}}z^6E_{11}(z)dz\\&A_{12}=\int_{-\frac{h}{2}}^{\frac{h}{2}}G_{12}(z)dz \qquad C_{12}=\int_{-\frac{h}{2}}^{\frac{h}{2}}z^2G_{12}(z)dz \qquad F_{12}=\int_{-\frac{h}{2}}^{\frac{h}{2}}z^4G_{12}(z)dz\end{aligned} \tag{15}$$

Using Eq. (14), the set of governing Eqs. (11) can be written as:

$$\begin{aligned}&A_{11}\frac{\partial^2 u}{\partial x^2}-c_1D_{11}\frac{\partial^3 w}{\partial x^3}+\left(B_{11}-c_1D_{11}\right)\frac{\partial^2\phi}{\partial x^2}-I_0\frac{\partial^2 u}{\partial t^2}+c_1I_3\frac{\partial^3 w}{\partial t^2\partial x}-J_3\frac{\partial^2\phi}{\partial t^2}=0\\&c_1D_{11}\frac{\partial^3 u}{\partial x^3}-c_1^2H_{11}\frac{\partial^4 w}{\partial x^4}+c_1\left(F_{11}-c_1H_{11}\right)\frac{\partial^3\phi}{\partial x^3}+\left(A_{12}-6c_1C_{12}+9c_1^2F_{12}\right)\left(\frac{\partial^2 w}{\partial x^2}+\frac{\partial\phi}{\partial x}\right)-\frac{P+Q-k_G}{b}\frac{\partial^2 w}{\partial x^2}\\&-\frac{k_w}{b}w-c_1I_3\frac{\partial^3 u}{\partial t^2\partial x}-I_0\frac{\partial^2 w}{\partial t^2}+c_1^2I_6\frac{\partial^4 w}{\partial t^2\partial x^2}-J_5\frac{\partial^3\phi}{\partial t^2\partial x}=0\\&\left(B_{11}-c_1D_{11}\right)\frac{\partial^2 u}{\partial x^2}-\left(c_1F_{11}-c_1^2H_{11}\right)\frac{\partial^3 w}{\partial x^3}+\left(C_{11}-2c_1F_{11}+c_1^2H_{11}\right)\frac{\partial^2\phi}{\partial x^2}-\left(A_{12}-6c_1C_{12}+9c_1^2F_{12}\right)\left(\frac{\partial w}{\partial x}+\phi\right)\\&-J_3\frac{\partial^2 u}{\partial t^2}+J_5\frac{\partial^3 w}{\partial t^2\partial x}-J_1\frac{\partial^2\phi}{\partial t^2}=0\end{aligned} \tag{16}$$

and boundary conditions at $x = L$ written in Eq. (13b) can be rewritten as follow:

$$\begin{aligned}
&x = L: \quad \frac{\partial u}{\partial x} = 0 \quad \frac{\partial^2 w}{\partial x^2} = 0 \quad \frac{\partial \phi}{\partial x} = 0 \\
&c_1 D_{11} \frac{\partial^2 u}{\partial x^2} - c_1^2 H_{11} \frac{\partial^3 w}{\partial x^3} + \left(c_1 F_{11} - c_1^2 H_{11}\right) \frac{\partial^2 \phi}{\partial x^2} + \left(A_{12} - 6c_1 C_{12} + 9c_1^2 F_{12}\right)\left(\frac{\partial w}{\partial x} + \phi\right) - \frac{Q - k_G}{b} \frac{\partial w}{\partial x} \\
&-c_1 I_3 \frac{\partial^2 u}{\partial t^2} + c_1^2 I_6 \frac{\partial^3 w}{\partial t^2 \partial x} - J_5 \frac{\partial^2 \phi}{\partial t^2} = 0
\end{aligned} \tag{17}$$

Using method of separation of variables as:

$$\{u(x,t) \quad w(x,t) \quad \phi(x,t)\} = \{U(x) \quad W(x) \quad \Phi(x)\} e^{\omega t} \tag{18}$$

The set of governing Eqs. (16) can be stated as follows:

$$\begin{aligned}
&A_{11} U'' - c_1 D_{11} W''' + \left(B_{11} - c_1 D_{11}\right) \Phi'' = \omega^2 \left(I_0 U - c_1 I_3 W' + J_3 \Phi\right) \\
&c_1 D_{11} U''' - c_1^2 H_{11} W'''' + \left(A_{12} - 6c_1 C_{12} + 9c_1^2 F_{12} - \frac{P + Q - k_G}{b}\right) W'' - \frac{k_w}{b} W + c_1 \left(F_{11} - c_1 H_{11}\right) \Phi''' \\
&+ \left(A_{12} - 6c_1 C_{12} + 9c_1^2 F_{12}\right) \Phi' = \omega^2 \left(c_1 I_3 U' + I_6 W - c_1^2 I_6 W'' + J_5 \Phi'\right) \\
&\left(B_{11} - c_1 D_{11}\right) U'' - c_1 \left(F_{11} - c_1 H_{11}\right) W''' - \left(A_{12} - 6c_1 C_{12} + 9c_1^2 F_{12}\right) W' + \left(C_{11} - 2c_1 F_{11} + c_1^2 H_{11}\right) \Phi'' \\
&- \left(A_{12} - 6c_1 C_{12} + 9c_1^2 F_{12}\right) \Phi = \omega^2 \left(J_3 U - J_5 W' + J_1 \Phi\right)
\end{aligned} \tag{19}$$

where prime indicates spatial derivation with respect x. Also, external boundary conditions (13a) and (17) can be written as:

$$x = 0: \quad U = 0 \quad W = 0 \quad W' = 0 \quad \Phi = 0 \tag{20a}$$

$$\begin{aligned}
&x = L: \quad U' = 0 \quad W'' = 0 \quad \Phi' = 0 \\
&c_1 D_{11} U'' - c_1^2 H_{11} W''' + \left(A_{12} - 6c_1 C_{12} + 9c_1^2 F_{12} - \frac{Q - k_G}{b}\right) W' + c_1 \left(F_{11} - c_1 H_{11}\right) \Phi'' + \left(A_{12} - 6c_1 C_{12} + 9c_1^2 F_{12}\right) \Phi \\
&= \omega^2 \left(c_1 I_3 U - c_1^2 I_6 W' + J_5 \Phi\right)
\end{aligned} \tag{20b}$$

It should be noted that in Eqs. (19) and (20), ω is a complex eigen value.

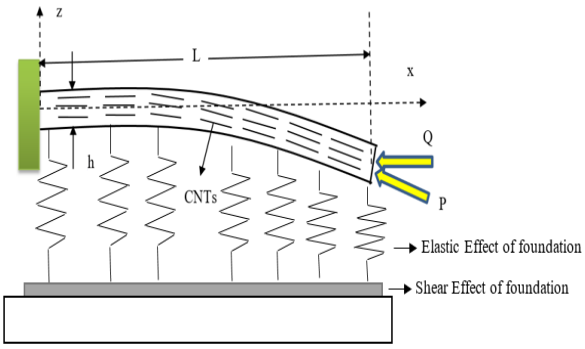

Fig.1
CNT-reinforced beam on Pasternak foundation subjected to axial and follower forces.

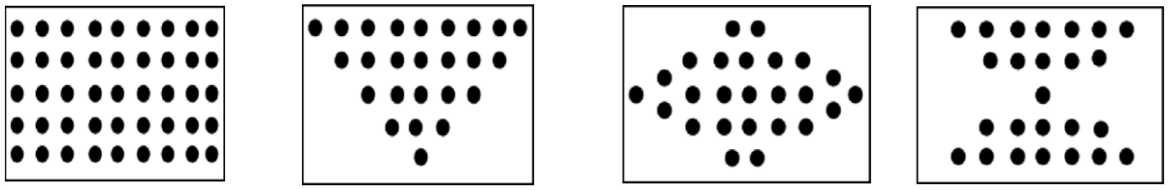

(a) UD (b) FG-V (c) FG-O (d) FG-X

Fig.2
Various linear distribution of CNTs.

3 DIFFERNTIAL QUADRATURE METHOD(DQM)

Differential quadrature method is based on the idea that all derivatives of a function can be easily approximated by means of weighted linear sum of the function values at *N* pre-selected grid of points as:

$$\left\{\frac{d^r f}{dx^r}\right\}_{N\times 1} = \left[A^{(r)}\right]_{N\times N} \{f\}_{N\times 1} \tag{21}$$

where $A^{(r)}$ is the weighting coefficient associated with the r^{th} order derivative given by [38]

$$A_{ij}^{(1)} = \begin{cases} \dfrac{\prod_{\substack{m=1\\ m\neq i,j}}^{N} (x_i - x_m)}{\prod_{\substack{m=1\\ m\neq j}}^{N} (x_j - x_m)} & i \neq j \\ \sum_{\substack{m=1\\ m\neq i}}^{N} \dfrac{1}{x_i - x_m} & i = j \end{cases} \qquad i,j = 1,2,3,\ldots,N$$
$$\left[A^{(r)}\right] = \left[A^{(1)}\right]\left[A^{(r-1)}\right] \quad 2 \le r \le N-1 \tag{22}$$

In this paper, for simplifying, following notations are considered:

$$[A] = \left[A^{(1)}\right] \quad [B] = \left[A^{(2)}\right] \quad [C] = \left[A^{(3)}\right] \quad [A] = \left[A^{(4)}\right] \tag{23}$$

Distribution of the grid points is an important aspect in convergence of the solution. A well-accepted set of the grid points is the Gauss–Lobatto–Chebyshev points given for interval [0,1] as [38]:

$$x_i = \frac{L}{2}\left\{1 - \cos\left[\frac{(i-1)\pi}{N-1}\right]\right\} \quad i = 1,2,3,...,N \tag{24}$$

4 DQ ANALOGUE

Using DQ rules, the set of governing Eqs. (19) can be written as:

$$[K]\{V\} = \omega^2 [M]\{V\} \tag{25}$$

In which

$$\{V\}=\begin{Bmatrix}\{U\}\\ \{W\}\\ \{\Phi\}\end{Bmatrix}\quad [K]=\begin{bmatrix}k_{11} & k_{12} & k_{13}\\ k_{21} & k_{22} & k_{23}\\ k_{31} & k_{32} & k_{33}\end{bmatrix}\quad [M]=\begin{bmatrix}m_{11} & m_{12} & m_{13}\\ m_{21} & m_{22} & m_{23}\\ m_{31} & m_{32} & m_{33}\end{bmatrix}$$

$$k_{11}=A_{11}[B]\quad k_{12}=-c_1D_{11}[C]\quad k_{13}=(B_{11}-c_1D_{11})[B]$$

$$m_{11}=I_0I\quad m_{12}=-c_1I_3[A]\quad m_{13}=J_3I$$

$$k_{21}=c_1D_{11}[C]\qquad k_{22}=-c_1^2H_{11}[D]+\left(A_{12}-6c_1C_{12}+9c_1^2F_{12}+\frac{k_G-P-Q}{b}\right)[B]-\frac{k_w}{b}I \tag{26}$$

$$k_{23}=c_1(F_{11}-c_1H_{11})[C]+(A_{12}-6c_1C_{12}+9c_1^2F_{12})[A]$$

$$m_{21}=c_1I_3[A]\quad m_{22}=I_0I-c_1^2I_6[B]\quad m_{23}=J_5[A]$$

$$k_{31}=(B_{11}-c_1D_{11})[B]\quad k_{32}=-c_1(F_{11}-c_1H_{11})[C]-(A_{12}-6c_1C_{12}+9c_1^2F_{12})[A]$$

$$k_{33}=(C_{11}-2c_1F_{11}+c_1^2H_{11})[B]-(A_{12}-6c_1C_{12}+9c_1^2F_{12})I$$

$$m_{31}=J_3I\quad m_{32}=-J_5[A]\quad m_{33}=J_1I$$

where I is identity matrix of order N. Also, external boundary conditions can be written as:

$$[T]\{V\}=\omega^2[R]\{V\} \tag{27}$$

In which

$$[T]=\begin{bmatrix}I_{1j} & \{0\} & \{0\}\\ \{0\} & I_{1j} & \{0\}\\ \{0\} & A_{1j} & \{0\}\\ \{0\} & \{0\} & I_{1j}\\ A_{Nj} & \{0\} & \{0\}\\ \{0\} & B_{Nj} & \{0\}\\ \{0\} & \{0\} & A_{Nj}\\ T_{81} & T_{82}-\dfrac{Q-k_G}{b}A_{Nj} & T_{83}\end{bmatrix}\quad [R]=\begin{bmatrix}\{0\} & \{0\} & \{0\}\\ \{0\} & \{0\} & \{0\}\\ \{0\} & \{0\} & \{0\}\\ \{0\} & \{0\} & \{0\}\\ \{0\} & \{0\} & \{0\}\\ \{0\} & \{0\} & \{0\}\\ \{0\} & \{0\} & \{0\}\\ c_1I_3I_{Nj} & -c_1^2I_6A_{Nj} & J_5I_{Nj}\end{bmatrix} \tag{28}$$

$$T_{81}=c_1D_{11}B_{Nj}\quad T_{82}=-c_1^2H_{11}C_{Nj}+(A_{12}-6c_1C_{12}+9c_1^2F_{12})A_{Nj}$$

$$T_{83}=c_1(F_{11}-c_1H_{11})B_{Nj}+(A_{12}-6c_1C_{12}+9c_1^2F_{12})I_{Nj}$$

In order to calculate the eigen values, Eqs. (25) and (27) should be solved. This simultaneous solution leads to create some redundant equations. So, governing equations in boundary points should be neglected [39, 40]:

$$[\bar{K}]\{V\}=\omega^2[\bar{M}]\{V\} \tag{29}$$

In which bar sign implies non-square matrix and boundary points are considered as:

$$\{V\}_b=\begin{Bmatrix}U_1\\ U_N\\ W_1\\ W_2\\ W_{N-1}\\ W_N\\ \Phi_1\\ \Phi_N\end{Bmatrix}=\begin{Bmatrix}V_1\\ V_N\\ V_{N+1}\\ V_{N+2}\\ V_{2N-1}\\ V_{2N}\\ V_{2N+1}\\ V_{3N}\end{Bmatrix} \tag{30}$$

Using Eqs. (27) and (29) following eigen value equation is obtained

$$[K_t]\{V\} = \omega^2 [M_t]\{V\} \tag{31}$$

where

$$[K_t] = \begin{bmatrix} \bar{K} \\ T \end{bmatrix} \quad [M_t] = \begin{bmatrix} \bar{M} \\ R \end{bmatrix} \tag{32}$$

Using Eq. (31) complex eigen values can be found. Imaginary part of these eigen values ($\Omega = Im(\omega)$) indicates to natural frequencies and real part shows stability of instability of the beam.

5 NUMERICAL RESULTS

In this section numerical results are presented for various cases. Convergence and accuracy of the presented solution are confirmed and a parametric study is presented on the effect of volume fraction and distribution of CNTs, geometrical parameters and stiffness coefficients of the foundation on the stability region.

Table 1
Efficiency parameters [41, 42].

V^*_{CNT}	η_1	η_2	η_3
0.12	0.137	1.022	
0.17	0.142	1.626	$0.7\eta_2$
0.28	0.141	1.585	

Unless otherwise stated, numerical results are presented for a beam made of Poly (methyl methacrylate), referred to as PMMA, as the matrix with material properties E^m = 2.5 *GPa*, ν^m = 0.34 and ρ^m = 1150 kg/m^3 and (10,10) armchair SWCNT (L = 9.26 *nm*, R = 0.68 *nm*, h = 0.067 *nm*) as the reinforcements. Elasticity moduli, shear modulus, Poisson's ratio and mass density of SWCNT are evaluated at reference temperature by Shen and Xiang [43] and are E_{11}^{CNT}= 5.6466 *TPa*, G_{12}^{CNT}= 1.9445 *TPa*, ν_{12}^{CNT}= 0.175 and ρ^{CNT}= 1400 kg/m^3. Results are presented for three different volume fractions of CNTs and corresponding values of efficiency parameters are presented in Table 1.

Unless otherwise stated, following values are considered:

$$L = 1m \quad b = 10cm \quad h = 5cm \quad V^*_{CNT} = 0.12 \quad k_w = 10^4 \frac{N}{m^2} \quad k_G = 10^3\, N$$

and following dimensionless parameters are defined:

$$\lambda = \omega L \sqrt{\frac{\rho_m}{E_m}} \quad P^* = \frac{P}{E_m L^2} \quad Q^* = \frac{Q}{E_m L^2} \quad k_w^* = \frac{k_w}{E_m} \quad k_G^* = \frac{k_G}{E_m L^2} \tag{33}$$

At first, convergence of the presented solution should be examined. For this purpose, consider a FG-X CNT reinforced beam subjected to Q = 2 *KN* and P = 5 *KN*. Table 2 shows effect of number of grid points on the real and imaginary parts of the eigen values for the first three modes. This table reveals that presented solution converges rapidly and for frequency the first three modes N = 13 is enough. This value is considered in all of the following examples.

Table 2
Convergence of the presented numerical solution (FG-X, $Q = 2$ *KN*, $P = 5$ *KN*).

N	$\Omega = Im(\lambda)$			$Re(\lambda)$		
	Mode 1	Mode 2	Mode 3	Mode 1	Mode 2	Mode 3
5	0.509449	9.532003	17.69614	-0.00191	-0.67316	-2.35182
7	0.369998	1.805542	3.658591	-0.00100	-0.02411	-0.09899
9	0.349563	1.699981	3.488799	-0.00090	-0.02137	-0.09000
11	0.342269	1.627437	3.385132	-0.00086	-0.01959	-0.08473
13	0.339901	1.567246	3.313810	-0.00085	-0.01863	-0.08217
15	0.340064	1.561887	3.310907	-0.00085	-0.01804	-0.08105

In order to validate the presented solution consider a CNT reinforced cantilever beam with no axial and follower forces, no foundation and the following properties [44]:

$$E_m = 2.5GPa,\ \upsilon^m = 0.3,\ \rho^m = 1190\frac{kg}{m^3}$$

$$E_{11}^{CNT} = 5646.6GPa,\ G_{12}^{CNT} = 1944.5GPa,\ \rho^{CNT} = 2100\frac{kg}{m^3}, \upsilon_{12}^{CNT} = 0.175,\ V_{CNT}^{*} = 0.17,$$

$$\eta_1 = 0.142,\ \eta_3 = 1.138,\ b = h = 10cm,\ L = 12h$$

For various types of CNTs distribution and first five modes of vibration, dimensionless values of the frequency are presented and compared in Table 3 with those reported by Lin and Xiang [44]. Comparison of results confirms high accuracy of the presented solution.

Consider a homogeneous beam of $L = 10$, b = 1 *m*, $h/L = 0.01$ with no axial force, no foundation and subjected to a follower force. In Fig. 3 effect of the dimensionless follower force ($\eta = 10^4 P/EA$, $A=bh$) on the real and imaginary parts of the first two dimensionless eigen values are depicted. As shown in this figure with increase in value of the follower force, first natural frequency increases and second one decreases. At a special value of the follower force (η= 1.645833) this two frequencies become equal to Ω = 0.031789 and corresponding value of the real part raise to positive values. In fact, at this point, oscillations of the beam become unstable which is known as flutter. Value of the follower force at this point is called critical follower force and the corresponding frequency is called the flutter frequency.

Table 3
First five dimensionless frequencies of a CNT-reinforced cantilever beam with no axial and follower forces and no foundation (E^m = 2.5 *GPa*, ν^m = 0.3, ρ^m = 1190 *kg/m*^{3}, E_{11}^{CNT} = 5.6466 *TPa*, G_{12}^{CNT}= 1.9445 *TPa*, ν_{12}^{CNT}= 0.175, ρ^{CNT}= 2100 *kg/m*^{3}, V_{CNT}^{*}=0.17, η_1= 0.142, η_3= 1.138, b=h=10 *cm*, L = 12h).

$\Omega^*=(\Omega L^2/h)(\rho_m/E_m)^{1/2}$	UD		FG-V		FG-X	
	Present	Lin and Xiang [44]	Present	Lin and Xiang [44]	Present	Lin and Xiang [44]
Mode 1	6.102602	6.16900	5.247523	5.30480	7.026457	7.10270
Mode 2	26.07763	25.4398	24.14084	23.5585	27.84940	27.2740
Mode 3	53.68519	53.3180	51.15805	50.8264	56.06942	55.7497
Mode 4	82.34153	81.1924	79.98986	78.8812	84.94143	83.9485
Mode 5	112.2116	110.8875	110.0281	108.6575	115.9162	114.5832

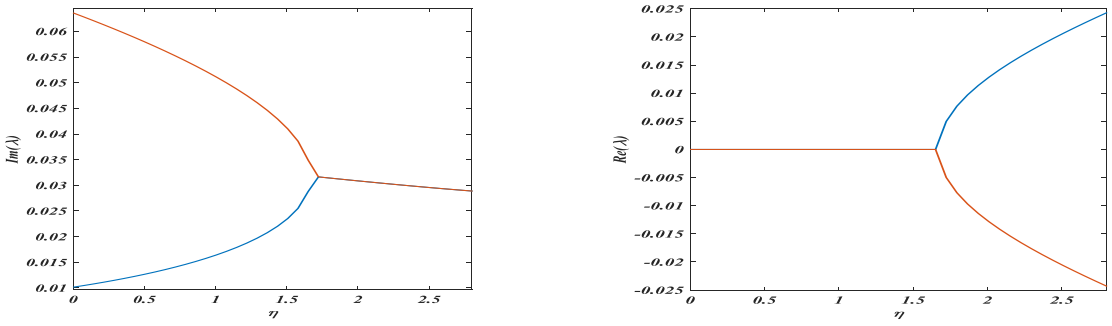

Fig.3
Effect of follower force on first two eigen values of beam.

Table 4
Critical follower force and flutter frequency of a homogeneous cantilever beam with no axial force and no foundation for various values of thickness to length ratio (L =10, b =1 m).

h/L	$\eta_{cr} = 10^4 P_{cr}/EA$			Ω_{cr}
	Presented	Djondjorov and Vassilev [16]	Difference (%)	Presented
0.01	1.645833	1.67	1.447126	0.031789
0.02	6.583333	6.66	1.151156	0.063433
0.03	14.81250	14.9	0.587248	0.094787
0.04	26.33333	26.4	0.252538	0.125711
0.05	40.49479	40.9	0.990733	0.156458
0.10	151.5625	154	1.582792	0.299502
0.15	311.7188	314	0.726497	0.419722
0.20	496.8750	497	0.025151	0.515590
0.25	678.7109	681	0.336138	0.589027
0.30	848.4375	855	0.767544	0.643789

For various values of thickness to length ratio, dimensionless values of the critical follower force and flutter frequency are presented in Table 4. Corresponding values of the critical follower force reported by Djondjorov and Vassilev [16] are presented at this table. Comparison of the results confirms high accuracy of the presented solution. In order to comparison of effect of the follower and axial forces a FG-X reinforced beam is considered. Effect of the axial or follower force on the first two dimensionless frequencies are shown in Fig. 4. According to this figure, critical value of the dimensionless follower force is about $P^*_{cr} = 5.385\times10^{-4}$. Fig. 4 reveals that with increase in value of the axial force, all frequencies decrease and in a special value of the axial force which is known as critical axial force ($Q^*_{cr} = 1.385\times10^{-4}$), frequency of the first mode drops to zero and beam become statically unstable. Comparison of critical values for follower and axial forces shows that the beam subjected to axial load (static instability) is closer to instability rather than the beam subjected to follower force (dynamic instability).

In what follows, a parametric study is presented to study effect of various parameters on the stability of the CNT-reinforced beam. In each figure, three diagrams are depicted:

- Value of the fundamental frequency versus value of the axial load (no follower force is applied).
- Values of the natural frequencies and corresponding real parts of the eigen values of the first two modes versus value of the follower force (no axial load is applied).
- Stability region for a beam subjected to both axial and follower forces.

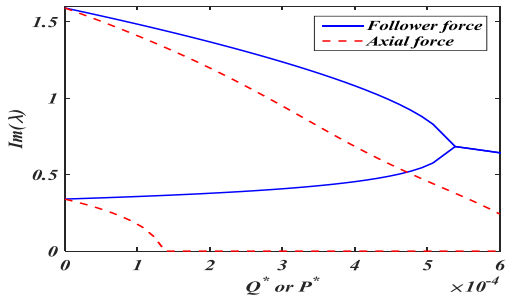

Fig.4
Effect of follower force on first two eigen values of beam.

In order to study effect of volume fraction of CNTs on the stability, a FG-X reinforced beam is considered. In Figs. 5(a)-5(c) effect of volume fraction of CNTs on the stability of the beam are shown. These figures shows that increase in volume fraction of CNTs leads to increase in both static and dynamic stability of the beam. In can be explained by high value of the elastic modulus of CNTs in comparison with elastic modulus of matrix. Fig. 5(b) shows that increase in volume fraction of CNTs increases flutter frequency

In order to study influence of distribution of CNTs on the stability, consider a FG-X reinforced beam. Effect of distribution of CNTs on the stability of the beam are depicted in Figs. 6(a)-6(c). These figures reveals that distribution of CNTs can be sorted in order to increase in stability of the beam as FG-X, UD, FG-V, FG-O. In other word, in order to get more stability, it is better to put CNTs far away from neural axis of the beam. Fig. 6(b) shows that distribution of CNTs can be sorted in order to increase in flutter frequency again as FG-X, UD, FG-V, FG-O.

In order to study effect of thickness of the beam on the stability, an FG-X reinforced beam is considered. For various values of thickness to length ratio, stability regions are depicted in Figs.7(a)-7(b). These figures show that thickness has a significant effect on the stability of the beam. It is shown that increase in thickness of the beam

expand stability regions and makes beam more stable. It should be noted that increase in thickness of the beam increases mass of the beam which should be considered as a disadvantage. Fig. 7(b) shows that increase in thickness of the beam increases flutter frequency.

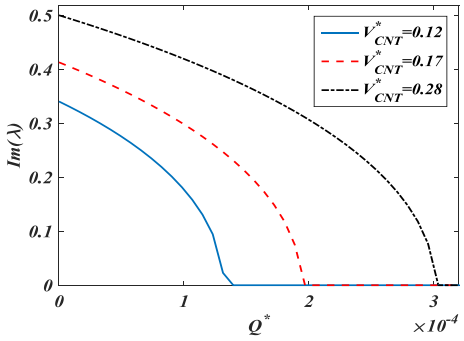

(a)Beam subjected to axial load

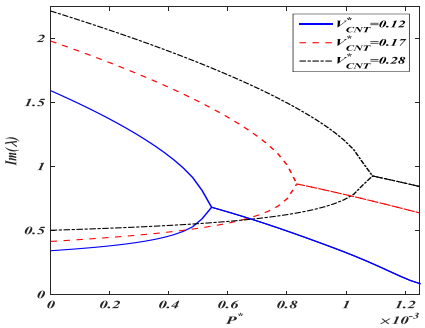

(b)Beam subjected to follower force

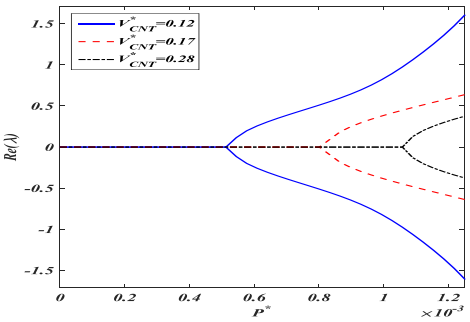

(b)Beam subjected to follower force

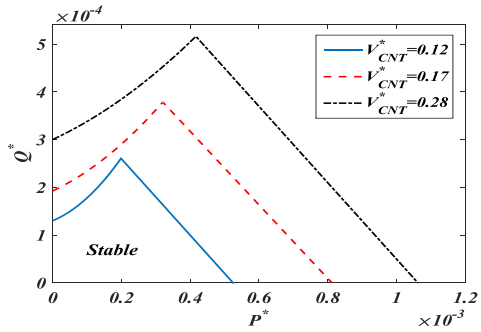

(c)Beam subjected to axial and follower forces

Fig.5
Effect of volume fraction of CNTs on the stability of the beam.

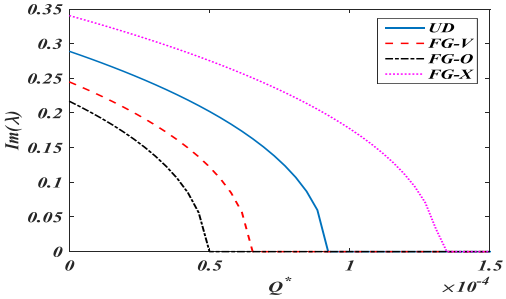

(a)Beam subjected to axial load

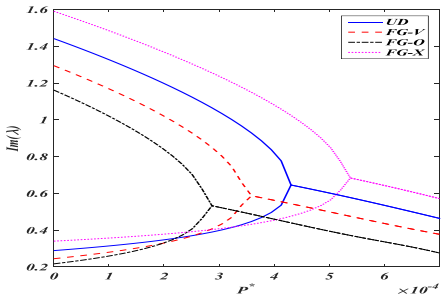

(b)Beam subjected to follower force

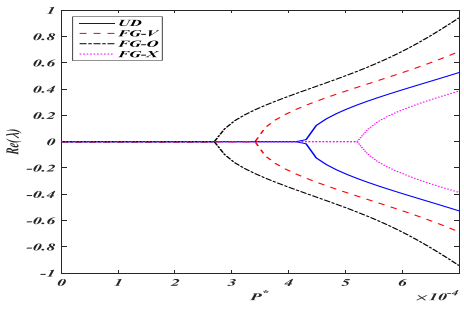

(b)Beam subjected to follower force

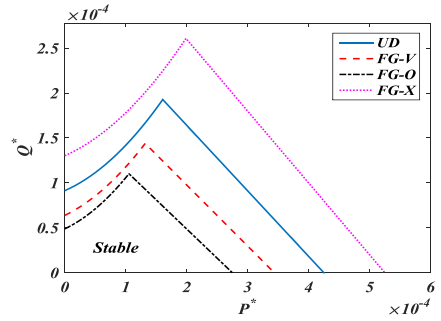

(c)Beam subjected to axial and follower forces

Fig.6
Effect of distribution of CNTs on the stability of the beam.

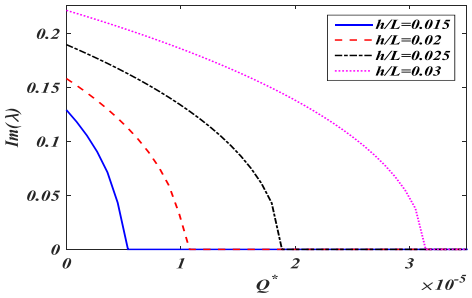

(a) Beam subjected to axial load

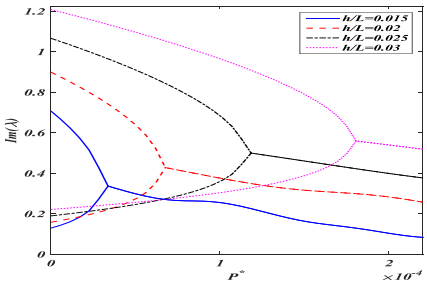

(b) Beam subjected to follower force

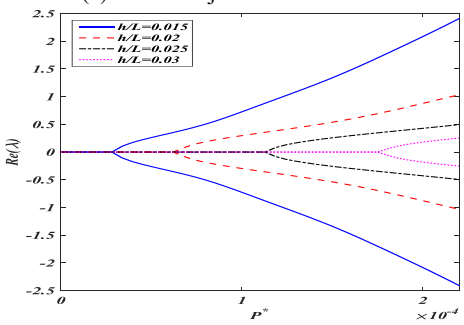

(b) Beam subjected to follower force

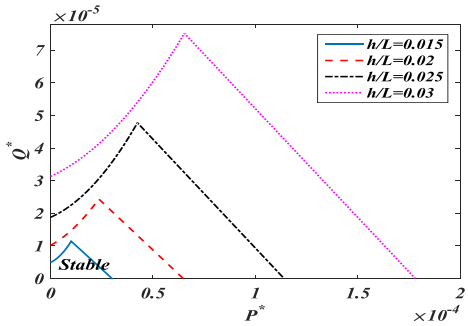

(c) Beam subjected to axial and follower forces

Fig.7
Effect of thickness to length ratio on the stability of the beam.

In order to study effect of width of the beam on the stability, consider a FG-X reinforced beam is considered. Figs.8(a)-8(b) stability regions are depicted for various values of width to length ratio. This figures show that like thickness, increase in width of the beam expand stability regions and makes beam more stable. A comparison between Figs. 7 and 8 reveals that thickness of the beam has more influence rather than width of the beam which is in agreement with $I = bh^3/12$. It can be stated that like thickness, increase in width of the beam makes beam heavier. Figs. 8(a) and 8(b) show that width of the beam has no significant effect on flutter frequency and when the beam is not subjected to axial or follower force, width of the beam has no effect on the natural frequencies.

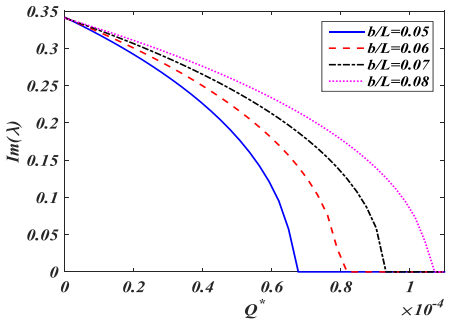

(a) Beam subjected to axial load

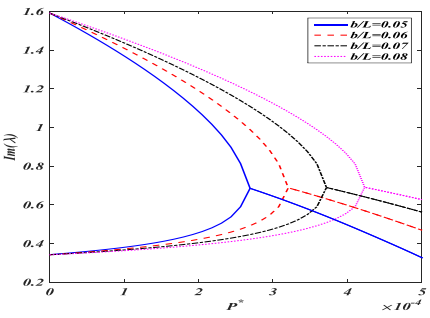

(b) Beam subjected to follower force

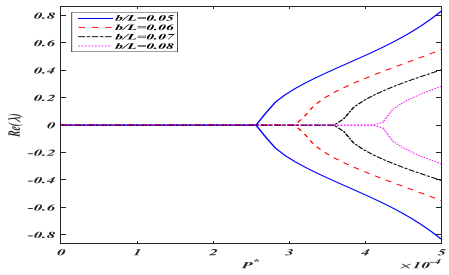

(b) Beam subjected to follower force

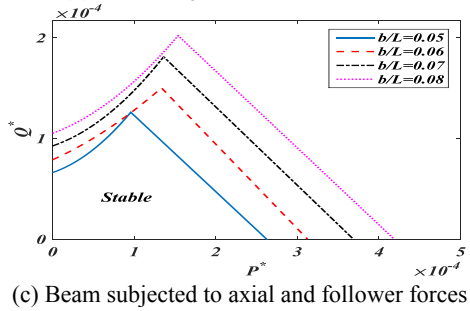

(c) Beam subjected to axial and follower forces

Fig.8
Effect of width to length ratio on the stability of the beam.

In order to study effect of elastic coefficient of the foundation on the stability of the beam, consider a FG-X reinforced beam. In Figs. 9(a)-9(c) effect of elastic coefficient of the foundation on the stability of the beam are depicted. These figures show that for a beam subjected to axial load, increase in elastic coefficient of the foundation increases critical load but for a beam subjected to follower force, this coefficient has no considerable effect on the critical follower force. Fig. 9(a) shows that increase in elastic coefficient of the foundation increases flutter frequency and decreases real parts of the eigen values in unstable regions which leads to decrease in amplitude of unstable oscillation of a fluttered beam.

In order to study effect of shear coefficient of the foundation on the stability of the beam, a FG-X reinforced beam is considered. Effect of shear coefficient of the foundation on the stability of the beam are depicted in Figs. 10(a)-10(c). These figures show that increase in elastic coefficient of the foundation expands stability regions and increase critical values of the axial or follower forces. Fig. 10(b) shows that a small increase in flutter frequency can be seen as shear coefficient of the foundation increases.

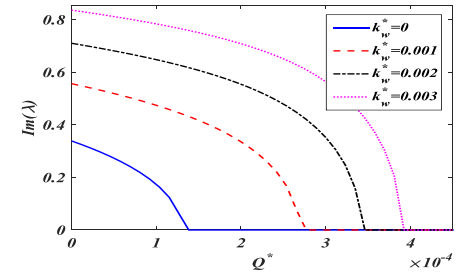

(a) Beam subjected to axial load

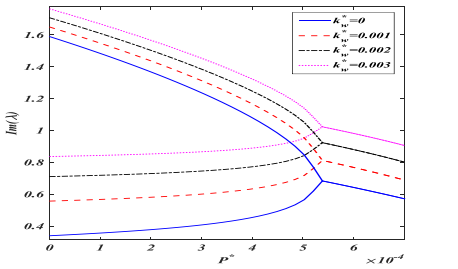

(b) Beam subjected to follower force

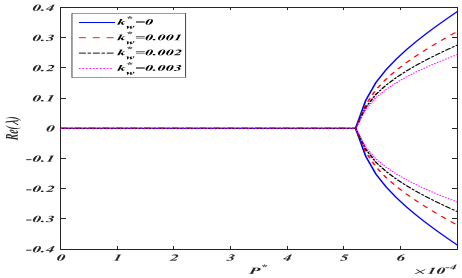

(b) Beam subjected to follower force

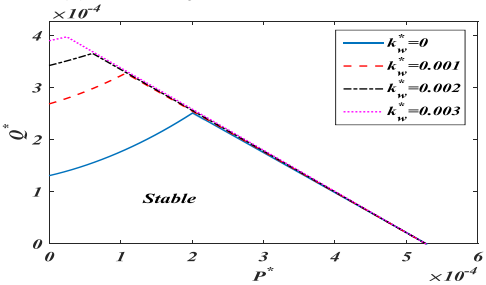

(c) Beam subjected to axial and follower forces

Fig.9
Effect of width to length ratio on the stability of the beam.

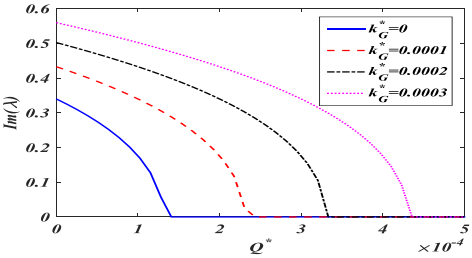

(a) Beam subjected to axial load

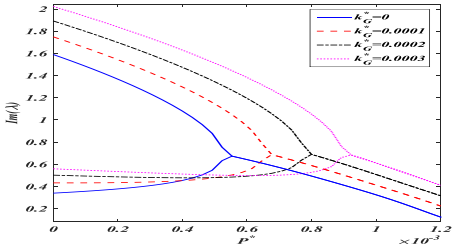

(b) Beam subjected to follower force

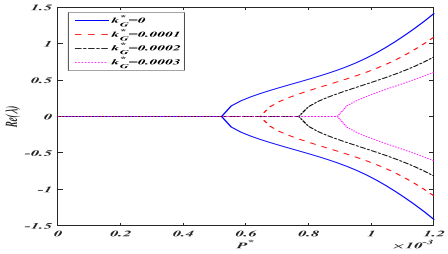

(b) Beam subjected to follower force

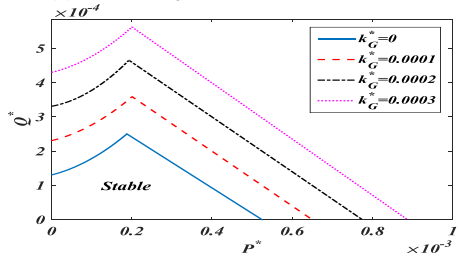

(c) Beam subjected to axial and follower forces

Fig.10
Effect of width to length ratio on the stability of the beam.

6 CONCLUSION

In this paper, differential quadrature method was employed and a numerical solution was presented for static and dynamic stability analysis of carbon nanotube (CNT) reinforced beams modeled based on the Reddy's third order shear deformation theory. The beam was subjected to compressive axial and follower and was resting on Pasternak foundation. Convergence and accuracy of the presented solution were confirmed and effect of various parameters on the stability region of the beam were investigated. Numerical results showed that increase in volume fraction of CNTs leads to a considerable enhancement in stability region. It was confirmed by numerical examples that among all pattern of distribution of CNTs, FG-X leads to the maximum expansion in stability regions. As was expected, it was shown by numerical results that increase in thickness and width of the beam and also shear coefficient of the foundation improve stability behavior of the beam subjected to both axial and follower forces. It was shown by numerical examples that increase in elastic coefficient of the foundation increases value of the critical axial load but it has no significant effect on the value of the critical follower force. Numerical examples revealed that increase in volume fraction of CNTs, thickness of the beam and elastic coefficient of the foundation and also using FG-X pattern for distribution of CNTs increase flutter frequency but width of the beam and shear coefficient of the foundation has no considerable effect on the flutter frequency.

REFERENCES

[1] Amabili M., Pellicano F., Païdoussis M., 1999, Non-linear dynamics and stability of circular cylindrical shells containing flowing fluid, Part II: large-amplitude vibrations without flow, *Journal of Sound and Vibration* **228**(5) :1103-1124.

[2] Amabili M., Pellicano F., Païdoussis M., 1999, Non-linear dynamics and stability of circular cylindrical shells containing flowing fluid. Part I: stability, *Journal of Sound and Vibration* **225**(4): 655-700.

[3] Amabili M., Pellicano F., Paidoussis M., 2000, Non-linear dynamics and stability of circular cylindrical shells containing flowing fluid. Part IV: large-amplitude vibrations with flow, *Journal of Sound and Vibration* **237**(4): 641-666.

[4] Amabili M., Pellicano F., Paidoussis M., 2000, Non-linear dynamics and stability of circular cylindrical shells containing flowing fluid. Part III: truncation effect without flow and experiments, *Journal of Sound and Vibration* **237**(4): 617-640.

[5] Afshari H., Torabi K., 2017, A parametric study on flutter analysis of cantilevered trapezoidal FG sandwich plates, *AUT Journal of Mechanical Enginerring* **1**(2): 191-210.

[6] Torabi K., Afshari H., 2017, Optimization for flutter boundaries of cantilevered trapezoidal thick plates, *Journal of the Brazilian Society of Mechanical Sciences Engineering* **39**(5): 1545-1561.

[7] Torabi K., Afshari H., Aboutalebi F.H., 2017, Vibration and flutter analyses of cantilever trapezoidal honeycomb sandwich plates, *Journal of Sandwich Structures Materials* **2017**: 1099636217728746.

[8] Torabi K., Afshari H., 2017, Materials, Optimization of flutter boundaries of cantilevered trapezoidal functionally graded sandwich plates, *Journal of Sandwich Structures* **2017**: 1099636217697492.

[9] Irie T., Yamada G., Takahashi I., 1980, Vibration and stability of a non-uniform Timoshenko beam subjected to a follower force, *Journal of Sound and Vibration* **70**(4): 503-512.

[10] Park Y., 1987, Dynamic stability of a free Timoshenko beam under a controlled follower force, *Journal of Sound and Vibration* **113**(3): 407-415.

[11] Lien-Wen C., Jeng-Ying Y., 1989, Nonconservative stability of a bimodulus beam subjected to a follower force, *Computers & Structures* **32**(5): 987-995.

[12] Lee H., 1996, Dynamic stability of a tapered cantilever beam on an elastic foundation subjected to a follower force, *International Journal of Solids and Structures* **33**(10): 1409-1424.

[13] Takahashi I., Yoshioka T., 1996, Vibration and stability of a non-uniform double-beam subjected to follower forces, *Computers & Structures* **59**(6): 1033-1038.

[14] Takahashi I., 1999, Vibration and stability of non-uniform cracked Timoshenko beam subjected to follower force, *Computers & Structures* **71**(5): 585-591.

[15] Young T., Juan C., 2003, Dynamic stability and response of fluttered beams subjected to random follower forces, *International Journal of Non-Linear Mechanics* **38**(6): 889-901.

[16] Djondjorov P.A., Vassilev V.M., 2008, On the dynamic stability of a cantilever under tangential follower force according to Timoshenko beam theory, *Journal of Sound and Vibration* **311**(3-5): 1431-1437.

[17] Goyal V.K., Kapania R.K., 2008, Dynamic stability of laminated beams subjected to nonconservative loading, *Thin-Walled Structures* **46**(12): 1359-1369.

[18] Li Q., 2008, Stability of non-uniform columns under the combined action of concentrated follower forces and variably distributed loads, *Journal of Constructional Steel Research* **64**(3): 367-376.

[19] Fazelzadeh S., Mazidi A., Kalantari H., 2009, Bending-torsional flutter of wings with an attached mass subjected to a follower force, *Journal of Sound and Vibration* **323**(1-2): 148-162.
[20] Wang L., 2012, Flutter instability of supported pipes conveying fluid subjected to distributed follower forces, *Acta Mechanica Solida Sinica* **25**(1): 46-52.
[21] Mao Q., Wattanasakulpong N., 2015, Vibration and stability of a double-beam system interconnected by an elastic foundation under conservative and nonconservative axial forces, *International Journal of Mechanical Sciences* **93**: 1-7.
[22] Bahaadini R., Hosseini M., Jamalpoor A., 2017, Nonlocal and surface effects on the flutter instability of cantilevered nanotubes conveying fluid subjected to follower forces, *Physica B: Condensed Matter* **509**: 55-61.
[23] Bahaadini R., Hosseini M., 2018, Flow-induced and mechanical stability of cantilever carbon nanotubes subjected to an axial compressive load, *Applied Mathematical Modelling* **59**: 597-613.
[24] Mohammadimehr M., Monajemi A.A., Afshari H., 2017, Free and forced vibration analysis of viscoelastic damped FG-CNT reinforced micro composite beams, *Microsystem Technologies* **26**(10): 3085-3099.
[25] Arefi M., Mohammad-Rezaei Bidgoli E., Dimitri R., Tornabene F., 2018, Free vibrations of functionally graded polymer composite nanoplates reinforced with graphene nanoplatelets, *Aerospace Science and Technology* **81**: 108-117.
[26] Arefi M., Mohammadi M., Tabatabaeian A., Dimitri R., Tornabene F., 2018, Two-dimensional thermo-elastic analysis of FG-CNTRC cylindrical pressure vessels, *Steel and Composite Structures* **27**(4): 525-536.
[27] Mohammadi M., Arefi M., Dimitri R., Tornabene F., 2019, Higher-order thermo-elastic analysis of FG-CNTRC cylindrical vessels surrounded by a pasternak foundation, *Nanomaterials* **9**(1): 79.
[28] Arefi M., Mohammad-Rezaei Bidgoli E., Dimitri R., Bacciocchi M., Tornabene F., 2019, Nonlocal bending analysis of curved nanobeams reinforced by graphene nanoplatelets, *Composites Part B: Engineering* **166**: 1-12.
[29] Arefi M., Zenkour A.M., 2017, Transient sinusoidal shear deformation formulation of a size-dependent three-layer piezo-magnetic curved nanobeam, *Acta Mechanica* **228**(10): 3657-3674.
[30] Arefi M., Mohammad-Rezaei Bidgoli E., Dimitri R., Bacciocchi M., Tornabene F., 2018, Application of sinusoidal shear deformation theory and physical neutral surface to analysis of functionally graded piezoelectric plate, *Composites Part B: Engineering* **151**: 35-50.
[31] Arefi M., Zenkour A.M., 2018, Thermal stress and deformation analysis of a size-dependent curved nanobeam based on sinusoidal shear deformation theory, *Alexandria Engineering Journal* **57**(3): 2177-2185.
[32] Arani A.G., Kiani F., Afshari H., 2019, Free and forced vibration analysis of laminated functionally graded CNT-reinforced composite cylindrical panels, *Journal of Sandwich Structures and Materials* **2019**: 1099636219830787.
[33] Arefi M., Zenkour A.M., 2019, Effect of thermo-magneto-electro-mechanical fields on the bending behaviors of a three-layered nanoplate based on sinusoidal shear-deformation plate theory, *Journal of Sandwich Structures and Materials* **21**(2): 639-669.
[34] Shen H.-S., 2009, Nonlinear bending of functionally graded carbon nanotube-reinforced composite plates in thermal environments, *Composite Structures* **91**(1): 9-19.
[35] Reddy J., 2007, Nonlocal theories for bending, buckling and vibration of beams, *International Journal of Engineering Science* **45**(2-8): 288-307.
[36] Sadd M.H., 2009, *Elasticity: Theory, Applications, and Numerics*, Academic Press.
[37] Rajesh K., Saheb K.M., 2017, Free vibrations of uniform timoshenko beams on pasternak foundation using coupled displacement field method, *Archive of Mechanical Engineering* **64**(3): 359-373.
[38] Bert C.W., Malik M., 1996, Differential quadrature method in computational mechanics: a review, *Applied Mechanics Reviews* **49**(1): 1-28.
[39] Lin R., Lim M., Du H., 1994, Deflection of plates with nonlinear boundary supports using generalized differential quadrature, *Computers & Structures* **53**(4): 993-999.
[40] Du H., Lim M., Lin R.,1995, Application of generalized differential quadrature to vibration analysis, *Journal of Sound and Vibration* **181**(2): 279-293.
[41] Shen H.-S., 2011, Postbuckling of nanotube-reinforced composite cylindrical shells in thermal environments, Part I: axially-loaded shells, *Composite Structures* **93**(8): 2096-2108.
[42] Mirzaei M., Kiani Y., 2016, Free vibration of functionally graded carbon nanotube reinforced composite cylindrical panels, *Composite Structures* **142**: 45-56.
[43] Shen H.-S., Xiang Y., 2014, Nonlinear vibration of nanotube-reinforced composite cylindrical panels resting on elastic foundations in thermal environments, *Composite Structures* **111**: 291-300.
[44] Lin F., Xiang Y., 2014, Vibration of carbon nanotube reinforced composite beams based on the first and third order beam theories, *Applied Mathematical Modelling* **38**(15-16): 3741-3754.